OPEN

Citation: Blood Cancer Journal (2013) 3, e156; doi:10.1038/bcj.2013.53

www.nature.com/bcj

ORIGINAL ARTICLE

A novel rapid-onset high-penetrance plasmacytoma mouse model driven by deregulation of cMYC cooperating with KRAS12V in BALB/c mice

Y Hu[1], M Zheng[2], R Gali[3], Z Tian[1], G Topal Görgün[1], NC Munshi[1], CS Mitsiades[1] and KC Anderson[1]

Our goal is to develop a rapid and scalable system for functionally evaluating deregulated genes in multiple myeloma (MM). Here, we forcibly expressed human cMYC and KRAS12V in mouse T2 B cells ($IgM^+B220^+CD38^+IgD^+$) using retroviral transduction and transplanted these cells into lethally irradiated recipient mice. Recipients developed plasmacytomas with short onset (70 days) and high penetrance, whereas neither cMYC nor KRAS12V alone induced disease in recipient mice. Tumor cell morphology and cell surface biomarkers ($CD138^+B220^-IgM^-GFP^+$) indicate a plasma cell neoplasm. Gene set enrichment analysis further confirms that the tumor cells have a plasma cell gene expression signature. Plasmacytoma cells infiltrated multiple loci in the bone marrow, spleen and liver; secreted immunoglobulins; and caused glomerular damage. Our findings therefore demonstrate that deregulated expression of cMYC with KRAS12V in T2 B cells rapidly generates a plasma cell disease in mice, suggesting utility of this model both to elucidate molecular pathogenesis and to validate novel targeted therapies.

Blood Cancer Journal (2013) **3,** e156; doi:10.1038/bcj.2013.53; published online 1 November 2013

Keywords: multiple myeloma (MM); cMYC; KRAS12V; retroviral transduction and transplantation; BALB/c mouse; plasmacytoma

INTRODUCTION

Multiple myeloma (MM) is a B-cell neoplasm characterized by accumulation of monoclonal plasma cells.[1] Neoplastic transformation in MM is associated with genomic and epigenetic dysregulation.[2] Previous studies have revealed that 40% of MM harbor chromosome translocations, including CCND1, CCND2, cMAF, MAFB and FGFR3/WHSC1, with immunoglobulin heavy chain (IgH).[3] Deletions of chromosome 13 are frequently detected in early and late stage MM.[4] During disease progression, genetic lesions accumulate, including mutations of NRAS and KRAS, overexpression of cMYC and downregulation of P53.[5] Using whole-genome sequencing and whole-exome sequencing,[6] more genetic lesions have been identified. Thus, it is critical to develop a short latency *in vivo* model to functionally evaluate the roles of these dysregulated genes in MM pathogenesis.

Mouse models both facilitate evaluation of the roles of genetic lesions detected in MM and provide for assessing therapeutic agents. The earliest mouse model for MM was induced by intraperitoneal injection of mineral oil, adjuvant and alkanes in BABL/c mice. These mice develop plasmacytomas at 200 days post injection;[7] however, plasmacytoma cells typically grow locally at the site of injection and rarely metastasize to bone marrow (BM). Widely used models now include xenograft models of MM generated by subcutaneous injection of human MM cell lines or primary human MM cells into SCID gamma mice. Particularly useful is the SCID-hu model, which is made by directly injecting MM cell lines or patient MM cells into human fetal bone implanted subcutaneously in SCID mice.[8] This model provides three-dimensional bone-like scaffolds to mimic the human MM microenvironment and has been used to both assess preclinical drugs and study MM pathogenesis. Another mouse model has been developed by transferring 5T2MM or 5T33MM mouse MM lines into syngeneic recipient mice. These mouse MM lines were established from aged C57BL/KaLwRij mice, which spontaneously develop a plasmacytoma with a low frequency and along with an osteolytic bone disease. These cells can be labeled with bio-trace marker, such as luciferase[9] or green fluorescent protein (GFP),[10] for *in vivo* imaging. A similar model was recently developed by intravenous injections of an *in vivo*-selected MOPC315 cell line into BALB/c mice.[11] Several transgenic mouse models have been developed based on expression of cMYC under control of an Ig light chain gene,[12] XBP-1,[13] cMAF[14] or cMYC[15] under the control of the Ig VH promoter and enhancer elements. These models recapitulate characteristics of MM; however, they are technically challenging and time consuming with long latency times and do not allow for evaluating multiple gene functions at a time.

A retroviral transduction/transplantation mouse model can overcome these limitations of transgenic mouse models as retroviral vectors can be used to overexpress or silence multiple gene(s) in target cells in a temporal sequence.[16] Retroviral transduction/transplantation mouse models have been widely used to study acute myeloid leukemia,[17] chronic myeloid leukemia,[18] B-cell acute lymphoid leukemia[19] and the majority of myeloproliferative neoplasms.[20] Based on previous studies,[12] we hypothesized that retroviral delivery of cMYC into a later stage B-cell subset might induce plasmacytomas in mice. MYC requires the cooperation or complementation with other oncogenes, such as v-H-ras or v-raf, for transformation.[21] We here therefore introduced KRAS (KRAS12V) mutation to complement the function of

[1]Department of Medical Oncology, LeBow Institute for Myeloma Therapeutics and Jerome Lipper Center for Multiple Myeloma Research, Dana-Farber Cancer Institute, Harvard Medical School, Boston, MA, USA; [2]Department of Pathology, Brigham and Women's Hospital, Boston, MA, USA and [3]C3 Bioinformatics Team, Countway Library, Harvard Medical School, Boston MA, USA. Correspondence: Dr KC Anderson, Department of Medical Oncology, LeBow Institute for Myeloma Therapeutics and Jerome Lipper Center for Multiple Myeloma Research, Dana-Farber Cancer Institute, Harvard Medical School, 450 Brookline Avenue, Boston, MA 02215, USA.
E-mail: kenneth_anderson@dfci.harvard.edu
Received 16 September 2013; accepted 24 September 2013

cMYC in tumorigenesis. With this strategy, we generated a rapid-onset high-penetrance plasmacytoma mouse model by enforced expression of cMYC and KRAS12V in later transition (T2) B-cell subset. This model provides a rapid tool to functionally evaluate genes in MM pathogenesis, as well as evaluate novel targeted therapies.

MATERIALS AND METHODS

DNA constructs

All PCR products were cloned into T-easy vector (Promega BioSystems, Sunnyvale, CA, USA) and completely sequenced to verify the correct reading frame.

To make a subclone vector MSCVm, MSCV-IRES-eGFP (MIG) was digested with BglII and CalI to remove IRES and eGFP, and ligased with an oligonucleotide (5′-GATCCGAATTCGTTAACGGATCCGGGCCCAAGCTTCAATT GGCGGCCGCAGATCTCTCGAGAT-3′) containing multiple clone sites, EcoRI, HpaI, BamHI, ApaI, HindII, MfeI, NotI, BglII, XhoI and ClaI.

Vector MIGm was constructed by introducing IRES-eGFP generated by PCR with a 5′ primer containing an EcroR1 and a 3′ primer containing a MfeI site into the MfeI site of MSCVm vector. MIGm-cMyc was generated by introducing cMYC released from MSCV-hcMYC-IRES-GFP vector (Addgene, Cambridge, MA, USA) with EcoRI into EcoRI site of MIGm vector. MIGm-KRAS12V was made by inserting KRAS12V obtained from T vector with NotI (blunt) and MfeI into MIGm vector disgested with EcoR1 and HpaI.

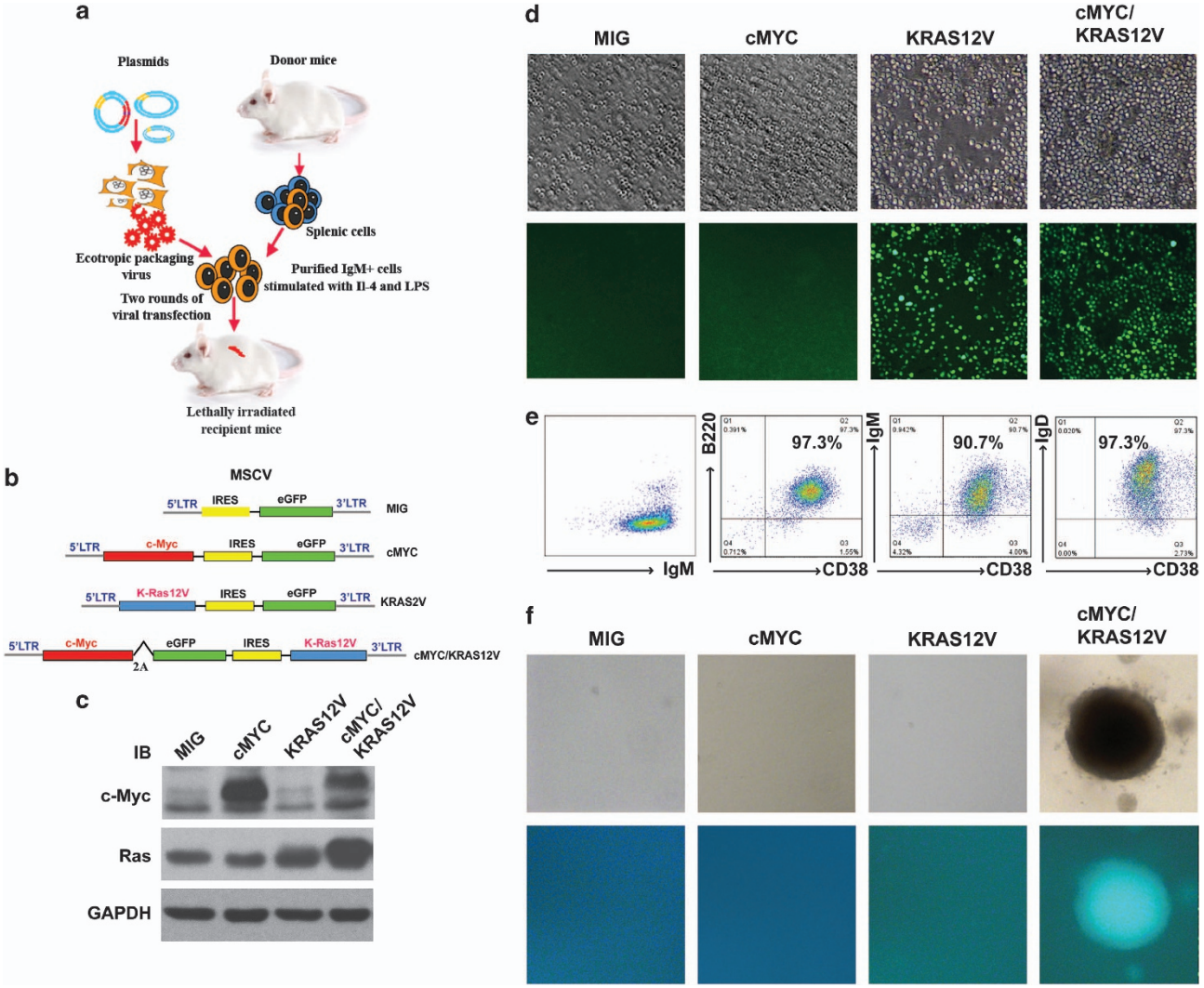

Figure 1. cMYC/KRAS12V can transform BaF3 cells independent of IL3 and transduce T2 B cells *in vitro*. (**a**) Workflow for generation of the adoptive plasmacytoma mouse model. (**b**) Schematic diagram of MSCV-based retroviral vectors: MIG, cMYC, KRAS12V and cMYC/KRAS12V. (**c**) Western blot analysis showed expression of MIG, cMYC, KRAS12V and cMYC/KRAS12V in transfected 293T cells. Total protein was analyzed against human MYC (upper) and RAS (middle); GAPDH (lower) served as a loading control. (**d**) KRAS12V and cMYC/KRAS12V drove BaF3 cells to grow independent of IL3 *in vitro*. Representative cells from two independent experiments are shown. (**e**) The purification of mouse IgM^+ spleen B cells after micro-bead isolation is shown (left panel). The cell population transited to T2 B-cell subset (IgM^+B220^+ $CD38^+IgD^+$) after stimulation with LPS and mIL4 for 48 h (right three panels). Assays were independently and repeatedly performed. (**f**) Colonies in methylcellulose assays were observed only in cells transduced by cMYC/KRAS12V but not other groups. Three independent experiments were performed.

Figure 2. cMYC/KRAS12V-induced plasmacytoma in BALB/c mice. (**a**) Recipients receiving MIG- or cMYC- or KRAS12V-transfected donor cells remained tumor free, whereas all recipients of cMYC/KRAS12V cells died with plasmacytomas. Secondary transplantation recipients of cMYC/KRAS12V-transduced tumor cells died with similar syndromes (2nd, secondary transplantation). Primary transplantation was repeated five times, and secondary transplantation was independently and repeatedly performed. Group sizes and survival times are indicated. (**b**) Tumor in peritoneal cavity and splenomegaly were observed in the cMYC/KRAS12V group animals ($n = 20$, from five independent experiments). (**c**) H&E staining showing tumor cell morphology ($n = 6$). (**d**) Tumor cells from peritoneal cavity (P.C.) and ascites (A.C.) ($n = 10$) were characterized as $CD138^+B220^-IgM^-GFP^+$ by flow cytometry.

MSCVm-cMYC-2A-eGFP-IRES-KRAS12V (MIKMG) was made by the following process: first, MSCVm was inserted a 2A sequence (5′-GATCCCAG CTGTTGAATTTTGACCTTCTTAAGCTTGCGGGAGACGTCGAGTCCAACCCCGGG CC-3′), which contains a BamHI and an ApaI competent site at 5′ and 3′ end, respectively; then, an eGFP coding sequence was inserted into MSCVm-2A vector, which was generated by PCR with a 5′ primer

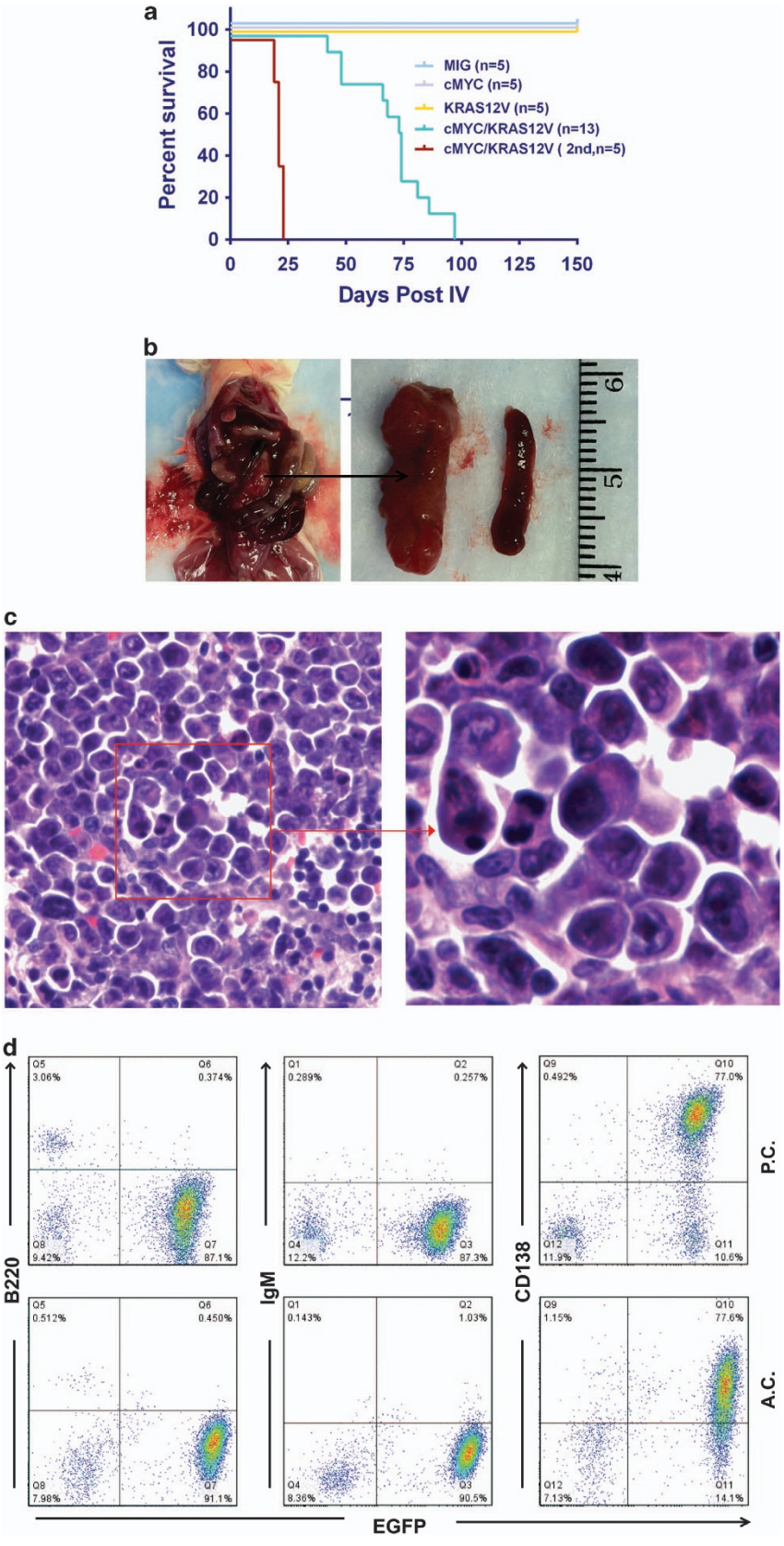

containing a ApaI site without its start code sequence and 3′ primer containing an MfeI site; next, IRES element was cloned into MSCVm-2A-eGFP vector at MfeI site, which was generated by PCR with a 5′ primer containing an EcoR1 site and 3′ primer containing an MfeI site; the open reading frame encoding cMYC generated by PCR from MIG-hcMYC vector (Addgene, 18119), with a 5′ primer containing an EcoR1 site and a

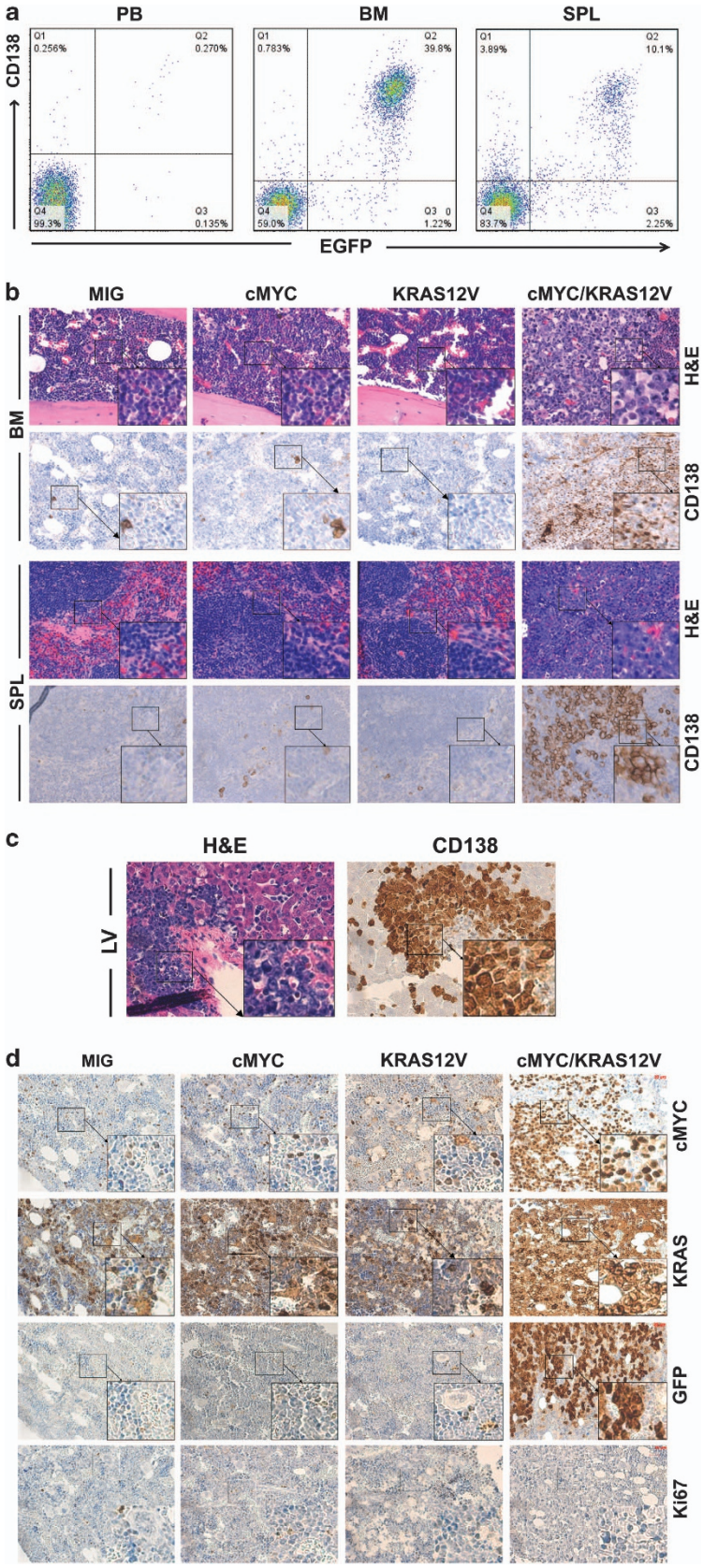

3′ primer containing a BamH1 site without stop coding sequence, was inserted into MSCVm-2A-eGFP-IRES with EcoRI and BamHI. KRAS12V open reading frame generated by PCR from pBabe-KRAS12V (Addgene, 12544) was cloned into MSCVm-cMYC-2A-eGFP-IRES with MfeI and NotI behind the IRES element.

Viral stock

All DNAs were purified in CsCl gradients. Lenti-X 293T cells (Clontech Laboratories, Mountain View, CA, USA) were co-transfected with 10 μg retroviral vector DNA and 5 μg pCL-Ecotropic packaging vector DNA using $CaCl_2$ method. Medium was changed at 24 h post transfection, and the supernatant was harvested at 48 h after transfection. Supernatant was filtered with 0.45-μm filters, aliquoted and frozen in a freezer at $-80\,^{\circ}C$. The virus titer was determined by transduction of NIH 3T3 cells, and the percentage of GFP^+ cells was screened by flow cytometry. After calculation, all viruses had titers $>4.8 \times 10^6$ GFP^+/ml.

Mouse IgM^+ B-cell isolation

All animal experiments were approved by and conformed to the standards of the Institutional Animal Care and Use Committee at the DFCI. BALB/c or C57BL/6J mice (The Jackson Laboratory, Bar Harbor, ME, USA; 000651) aged 6–12 weeks were used in all experiments. Mice were killed by CO_2 asphyxiation. Mouse IgM^+ splenic B cells were isolated using magnetic microbeads and LS MACS separation columns (Miltenyi Biotec, Cambridge, MA, USA).

Retroviral transfection and transplantation

IgM^+ cells were counted and plated at 2×10^7 cells per 10-cm plate in pre-stimulation medium of RPMI1640 containing 15% (vol/vol) inactivated fetal calf serum, 1% (vol/vol) penicillin/ streptomycin, 1.0 μg/ml ciprofloxacin, 200 μM l-glutamine, 10 ng/ml recombinant murine interleukin 4 (mIL4; Sigma, St Louis, MO, USA), and 50 μg/ml lipopolysaccharide (LPS; Sigma). After pre-stimulation for 24 h, viable cells were counted and transduced with retroviral stocks in the same medium containing 50% retroviral supernatant, 10 mM Hepes, pH 7.4 and 2 μg/ml polybrene. To increase transduction efficiency, virus and cells were cosedimented at 1000 *g* for 90 min in a Sorvall RT-5.3 centrifuge. Medium was changed after a 3-h adsorption period. On the next day, a second round of transduction and cosedimentation was performed using the same conditions. After another 3 h, cells were harvested and 5×10^5 cells were injected via the lateral tail vein with 5×10^5 BM into lethally irradiated recipients.

In vitro proliferation and differentiation assays

For colony assay, 1×10^5 transfected cells in 100 μl were mixed with 3 ml HSC-CUF basic media (Miltenyi Biotec, 130-091-275) in 15-ml tube. Cells were transferred into six-well cell culture plates with 16-gauge blunt-end needles (Miltenyi Biotec, 130-091-558), and the plate's interspace was filled with 10 ml sterilized phosphate-buffered saline (PBS) to maintain humidity of the culture environment. Cells were cultured at $37\,^{\circ}C$ and 5% CO_2 for 2 weeks.

Histopathology and immunohistochemistry (IHC)

Tissues were fixed, processed, sectioned and stained with hematoxylin-eosin by routine methods. Femurs were additionally treated for 1 h in decalcifying solution (Fisher Scientific, Cambridge, MA, USA). IHC was performed according to the standard procedures using rat anti-mouse CD45R/B220 (RA3-6B2) and rat anti-mouse CD138 (281-2) monoclonal antibodies obtained from BD Biosciences; anti-cMYC, RAS and eGFP antibodies obtained from Cell Signaling (Franklin Lakes, NJ, USA); as well as goat anti-mouse polyclonal antibodies for IgH chains IgA, IgM, IgG and kappa or lambda light chains conjugated to horseradish peroxidase (Southern Biotechnology, Birmingham, AL, USA).

Flow cytometry

Red blood cells were removed from single-cell suspensions of peripheral blood, BM, peritoneal fluid and spleen by RBC lysis buffer. Cells were then washed once with PBS and stained for 15 min at room temperature with the combination of the following antibodies: IgM-PE, B220-PECy7, CD138-APC, CD38-PE and IgD-PE washing once with PBS, and then cells were analyzed on a FACScalibur machine (Becton Dickinson, Franklin Lakes, NJ, USA) using Cell Quest software (Becton Dickinson).

Western blots

Whole-cell extracts from target cells were prepared, electroblotted onto NC membranes (Amersham, Wilson, OK, USA) and probed with primary antibodies according to the standard procedures. The anti-cMYC, RAS and eGFP antibodies were obtained from Cell Signaling. Following incubation with horseradish peroxidase-conjugated goat anti-rabbit or anti-mouse secondary antibody (Cell Signaling, Danvers, MA, USA), bound Igs were detected using ECL detection solutions (Pierce, Rockford, IL, USA). Anti-GAPDH served as a loading control.

Southern blot analysis of the IgH gene

Genomic DNA was prepared from IgM + B cells or cMYC/KRAS12V-induced plasmacytoma cells with Qiagen DNeasy 96 Blood and Tissue Kit (Qiagen, Valencia, CA, USA). DNA was digested with EcoRI. Blots were hybridized with a JH4 probe of the mouse IgH locus. The JH4 probe was generated by PCR using a plasmid containing a 1.9 BamHI-EcoRI genomic fragment of mouse heavy-chain locus as template and primers JH4f (5′-TACTATGC-TATGGACTACTGG-3′) and JH4r (5′-CTCTCCAGTTTCGGCTGAATC-3′). Southern blot hybridization was performed as described.[22]

Gene expression profiling

RNA from purified IgM^+ B cells and plasmacytoma cells was extracted with RNA mini kit (Grand Island, NY, USA), and gene expression profiling was performed using the Affymetrix mouse 430A2.0 gene chip (Affymetrix, Cleveland, OH, USA). Microarray data were analyzed with OneChannelGUI package in R workplace. Differential expression was determined using the LIMMA model. Gene signatures were analyzed with gene set enrichment analysis (GSEA) in Molecular Signatures Database (MSigDB).

RESULTS

Design of multiple gene expression MSCV-based vectors

To develop an adoptive mouse plasmacytoma model, we purified splenic IgM^+ B cells, which were cultured with LPS and mIL4 for 24 h. These target cells were transfected twice within 24 h and then injected via tail vein (intravenous) into lethally irradiated syngeneic recipients (Figure 1a). To develop oncogene expression vectors, we modified the retroviral vector MIG (MSCV-IRES-eGFP) by inserting multiple cloning sites. We constructed three oncogene expression vectors: cMYC (5′LTR-cMYC-IRES-eGFP-3′LTR), KRAS12V (5′LTR-KRAS12V-IRES-eGFP-3′LTR) and cMYC/KRAS12V (5′LTR-cMYC-2a-eGFP-IRES-KRAS12V-3′LTR). All oncogenes are driven by the cytomegalovirus type I enhancer and the mouse sarcoma virus promoter within the 5′ LTR (long terminal repeat; Figure 1b). Target genes were efficiently expressed by the vectors in transiently transfected 293T cells (Figure 1c).

To investigate the biological and functional sequelae of these oncogenes, we transfected BaF3 cells with MIG, cMYC, KRAS12V or cMYC/KRAS12V. Two days after transfection, GFP^+ cells were sorted and cultured without IL3. After a week, both KRAS12V and cMYC/KRAS12V, but not cMYC or MIG alone, drove BaF3 cells growth *in vitro* independent of IL3 (Figure 1d). These data suggest

Figure 3. Plasmacytoma cells infiltrated multiple organs. (**a**) Flow cytometry analysis of GFP and CD138 to track tumor cells in peripheral blood (PB), femur and tibia BM and spleen (SPL). Numbers represent tumor cell percentage in respective gates. Samples ($n = 25$) of individual mice from different experiments were analyzed. (**b**) BM and spleen (SPL) sections from mice receiving MIG-, cMYC-, KRAS12V- and cMYC/KRAS12V-transfected cells were stained with hematoxylin-eosin (H&E) and anti-CD138 antibody to identify plasmacytoma cells. (**c**) Liver (LV) sections from diseased mice were stained with H&E (left) and anti-CD138 antibody (right). (**d**) IHC analysis of BM sections showed expression of cMYC, KRAS and eGFP in cMYC/KRAS12V-induced plasmacytoma cells.

that KRAS12V has the capacity to suppress cMYC-induced apoptosis in BaF3 cells.

Previous studies have shown that overexpression of oncogenes cMYC, cMAF and XBP-1 driven by Eμ promoter in immature B cells induces plasma cell neoplasms in mice.[12–15] Here we used T2 B-cell subset ($IgM^+B220^+CD38^+IgD^+$)[23] as target cells, which are generated from stimulating purified IgM^+ B cells with LPS and mIL4 for 48 h (Figure 1e). To determine whether cMYC-, KRAS12V- or cMY/KRAS12V-transfected cells could grow *in vitro*, we performed soft agar colony assays. T2 B cells transfected with MIG, cMYC, KRAS12V or cMYC/KRAS12V were seeded in soft agar culture media, and after 2 weeks, only cMYC/KRAS12V-transduced cells formed colonies *in vitro* (Figure 1f). These results suggested that cMYC/KRAS12V had the capacity to promote independent T2 B cells growth *in vitro*.

cMYC/KRAS12V induced plasmacytomas in BALB/c mice

To determine whether cMYC/KRAS12V can transform T2 B cells and induce plasmacytomas *in vivo*, we transplanted T2 B cells transfected with MIG, cMYC, KRAS12V or cMYC/KRAS12V into lethally irradiated syngeneic recipient mice. Only mice that received cMYC/KRAS12V-transfected T2 B cells developed fatal tumors within 10 weeks post transplantation (Figure 2a). In diseased mice, peritoneal tumor, splenomegaly, and ascites were noted (Figure 2b). Tumor cells had dispersed nuclear chromatin, a low nuclear-to-cytoplasmic ratio and amphophilic cytoplasm with paranuclear hof. Binucleate cells and mitoses were rarely observed (Figure 2c). The analyses by flow cytometry showed tumor cell surface positivity for GFP and CD138, but absence of IgM and B220 ($CD138^+B220^-IgM^-GFP^+$) (Figure 2d). These features and phenotypes resemble previously reported transgenic and chemically induced plasmacytoma mouse models.[24,25] We also tested whether cMYC/KRAS12V-transformed plasmacytoma cells could cause similar tumors in secondary transplant recipients. In these experiments, splenic tumor cells from diseased mice were transferred into syngeneic mice, and all recipients developed tumors within 4 weeks (Figure 2a).

In chemically induced plasmacytoma mouse models, plasmacytoma cells are typically located at the site of injection and infrequently metastasize to BM and other organs.[26,27] In MM patients, tumor cells frequently affect BM and kidney, but rarely directly infiltrate other organs. To further define the anatomic distribution of plasmacytoma cells in our model, cells isolated from the peripheral blood, BM and spleen were analyzed for eGFP and CD138 expression. We found that plasmacytoma cells infiltrated BM (30–50%) and spleen (10–70%) and, to a lesser ($\leqslant$ 0.3% of total cells) extent, in peripheral blood (Figure 3a). Only cMYC/KRAS12V mice developed plasmacytomas with tumor cell infiltration in the BM and spleen. All tumor cells have similar cell morphology and surface phenotype (Figures 3b and c).

To determine the contribution of cMYC and KRAS12V in plasmacytoma development, we performed IHC assays with antibodies specific for cMYC, KRAS and GFP on BM specimens. Positive staining for cMYC, KRAS and GFP were confirmed in plasmacytoma cells within tissues from cMYC/KRAS12V, but not MIG, cMYC or KRAS12V, mice (Figure 3d).

Hypergammaglobulinemia, renal and bone alterations in diseased mice

A characteristic feature of MM and other plasma cell neoplasms is secretion of monoclonal Ig, detected as a distinct band (M-spike) by serum protein electrophoresis. In our model, M-spikes were detected in both the serum and ascites in cMYC/KRAS12V mice, but not in the serum of others (MIG, cMYC and KRAS12V) (Figure 4a and data not shown). The Ig chain isoforms in diseased mice include IgG1, IgM and IgA heavy chains and both of κ and λ light chains (Figure 4b). Southern blot analysis of IgH gene rearrangement in plasmacytoma cells indicated that cMYC/KRAS12V-induced plasmacytomas were clonal (Figure 4c).

In human MM, development of Ig heavy and light chain, as well as infiltration of tumor cells, leads to both renal tubular obstruction and glomerular damage. We observed glomerular shrinkage in cMYC/KRAS12V mice but not in other groups (Figure 5a). These renal lesions were similar to pathological manifestations in MM.[28] To assess Ig deposition, we performed IHC assays with antibodies specific for mouse Igs IgG, IgM, κ and λ. Ig chains were deposited in both the tubules and glomerulus (Figure 5b).

Another hallmark of human MM is osteolytic bone lesions. To determine whether the bone lesions developed in diseased mice, we examined bone structure changes with micro-computed tomography (micro-CT). No bone osteolysis was detected, even in the cMYC/KRAS12V group mice (Figure 5c).

Gene expression profiling in cMYC/KRAS12V-induced plasmacytoma cells

To gain further insights into the roles of cMYC/KRAS12V in tumorigenesis and identify the tumor type, we analyzed the gene expression signatures of cMYC/KRAS12V-induced tumor cells by using global transcriptional profiling analysis and comparing tumor cells to syngeneic murine IgM^+ B cells. Genes were considered significantly altered based on more than twofold change in mean expression ($P<0.05$). Using these criteria, 4466

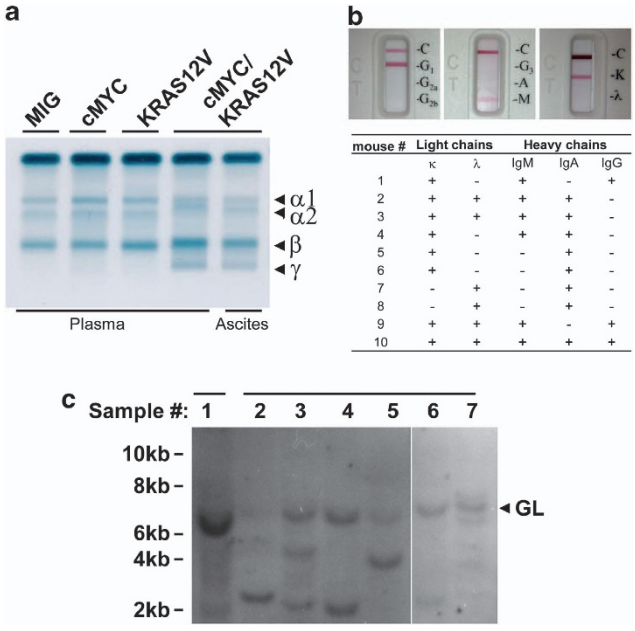

Figure 4. Evidence of clonality and hypermutation of expressed Ig genes in cMYC/KRAS12V-induced plasmacytoma mice. (**a**) Serum protein electrophoresis (SPEP) in serum and ascites from cMYC/KRAS12V-induced plasmacytoma mice. The bands are indicated with arrows. Samples were obtained from all the group animals as labeled ($n=5$ each group). (**b**) Ig isoform identification. Ascites were collected from plasmacytoma mice and analyzed with Thermo Scientific Pierce Rapid ELISA Mouse mAb Isotyping Kit. The Ig isoforms ($n=10$) are represented by color labeled bands as indicated. (**c**) Southern blot analysis for clonotypic IgH -chain rearrangement in plasmacytoma cells. Genomic DNA was isolated from IgM^+ B cells (sample 1) or cMYC/KRAS12V-induced plasmacytoma cells (samples 2–7), digested with EcoRI restriction enzyme and hybridized with murine JH4 probe. GL denotes germline band.

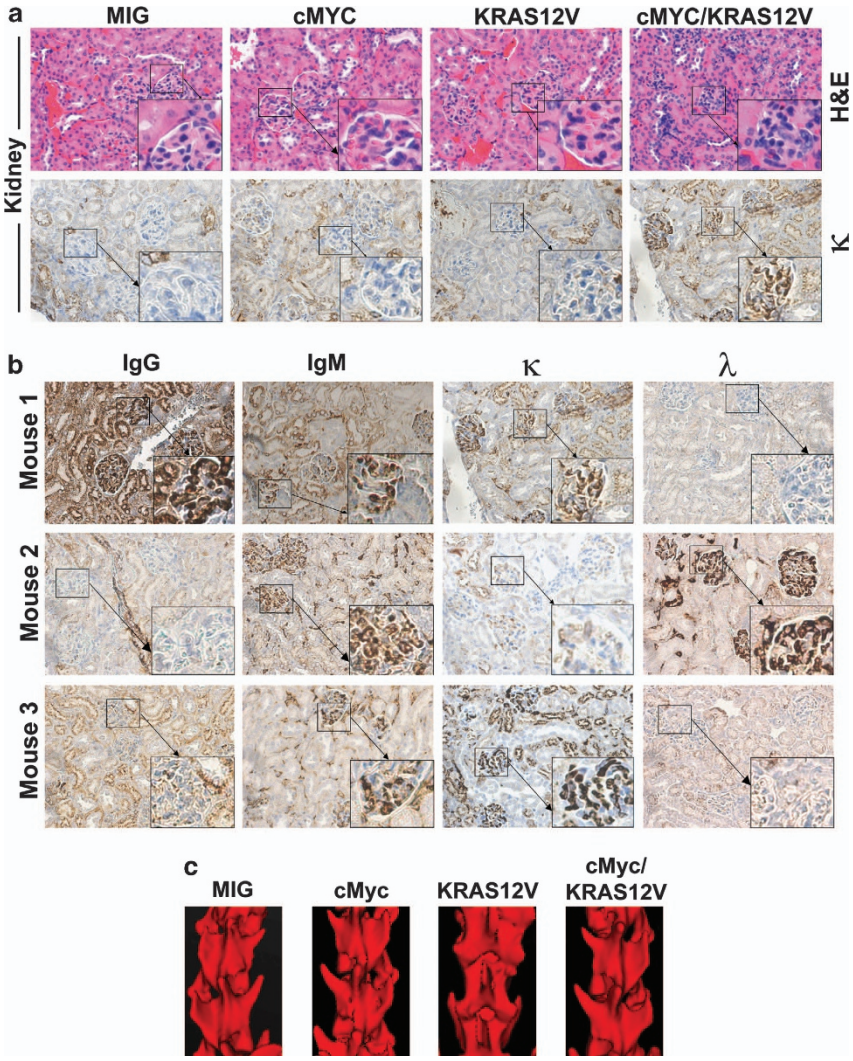

Figure 5. Renal and bone alterations in cMYC/KRAS12V-induced plasmacytoma mice. (**a**) Renal tissue from mice receiving MIG-, cMYC-, KRAS12V- and cMYC/KRAS12V-transfected cells ($n = 3$ each group) were analyzed by light microscopy (hematoxylin-eosin staining) and IHC staining with antibodies against mouse Ig κ chains. (**b**) Histological sections of kidneys of mice receiving cMYC/KRAS12V-transduced plasmacytomas were analyzed by IHC staining with antibodies against mouse Ig κ and λ light chains, as well as IgG and IgM heavy chains. (**c**) Micro-CT analysis demonstrated no bone lesions in all the group animals. Representative graphs from three individual animals are shown.

genes were significantly altered in tumor cells: 2333 were upregulated and 2133 were downregulated. Transcription factors required for plasma cell differentiation and survival were significantly increased: PRDM1 (Blimp-1), IRF4 and XBP-1 were increased 5.9-, 4.8- and 3.6-fold, respectively. Conversely, B-cell transcription factors absent or downregulated in plasma cells, including BCL-6, CIITA, MTA3, EBF1, STAT3, PAX5 and SPIB, were also significantly downregulated in plasmacytoma cells (Supplementary Data, Supplementary Table S1). Expression of several hallmark plasma cell differentiation and survival genes were confirmed using quantitative real-time PCR (Figure 6a). GSEA also revealed significant enrichments for upregulation of genes related to plasma cell differentiation and survival (Figure 6b, Supplementary Figure S1A), whereas gene sets related to B-cell receptor signaling were downregulated (Figure 6d). As expected, genes regulated by IRF4 and XBP1 were significantly upregulated (Figure 6e and Supplementary Figures S1B and C). Finally, several components of the nuclear factor-κB (NF-κB) pathways, including NF-κB1 and NF-κB2, and Rel, RelA and RelB were also downregulated in tumor cells (Figure 6f and Supplementary Figure S1D). These data are consistent with previous comparison of plasma cells versus IgM^+ B cells.[29–32]

To confirm the functional roles of cMYC and KRAS12V in plasmacytoma genesis, we performed GSEA with four well-established canonical transcriptional signatures of MYC-dependent genes.[26,33–35] Most genes in these gene sets were significantly upregulated in plasmacytoma cells (Figure 7a and Supplementary Figure S2A). Previous studies have demonstrated that RAS suppressed cMYC-induced apoptosis via activating PI3K/AKT pathway.[36] Activated AKT in turn phosphorylates and activates mammalian target of rapamycin (mTOR), an essential component of mTORC1 that promotes tumor cell proliferation and survival.[37] In cMYC/KRAS12V-transduced plasmacytoma cells, genes in mTOR target gene set[38] were significantly upregulated (Figure 7b and Supplementary Figure S2B). These results further confirm the formation of plasmacytoma due to cooperation of cMYC and KRAS12V. As in other tumors, genes regulating cell cycle,[39] as well E2F[40] target genes, and genes suppressed by RB1[41] were also significantly upregulated (Supplementary Figure S2C). Apoptotic signaling was inhibited by cMYC/KRAS12V: specifically, genes suppressed by P53 and P73 during cell growth arrest and apoptosis were enriched and upregulated in plasmacytoma cells (Figure 7c and Supplementary Figure S2C). Several other gene sets were also enriched and upregulated plasmacytoma cells, including

a **Confirmation of selected microarray result by quantitative RT-PCR**

Gene name	Accession number	Microarray results, mean fold change: PI/IgM-B	RT-PCR, C_T average, PI	RT-PCR, C_T average, IgM-B	RT-PCR results, fold change: PI/IgM-B
Prdm1	NM_007548	5.882	20.797	25.752	35.403
Irf4	NM_013674	2.265	15.369	19.845	24.702
		4.775			
Xbp-1	NM_001271730	2.705	15.99	21.187	39.911
		4.011			
		4.181			
Pax5	NM_008782	-2.014	25.954	18.757	-157.27
Bcl6	NM_009744	-44.742	24.979	21.311	-13.93
		-3.294			
Spib	NM_019866	-182.157	25.308	19.413	-70.508

PI indicates plasmacytoma cells; IgM-B indicates IgM postive B cells
CT indicates cycle number at which DRn corosses the threshold for the sample

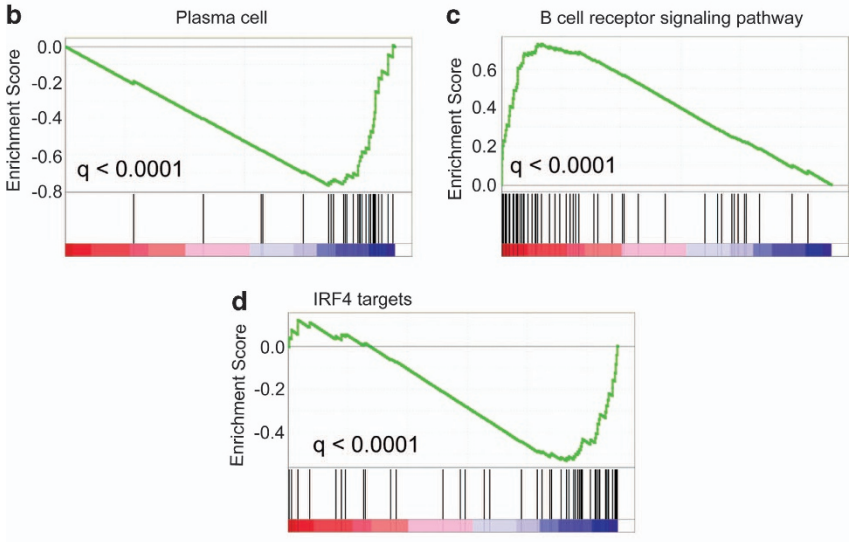

e

Gene Set	SIZE	NES	FDR q-val
MORI_PLASMA_CELL_UP	33	-1.50	< 0.0001
TARTE_PLASMA_CELL_VS_B_LYMPHOCYTE_UP	65	-1.18	0.17922
TARTE_PLASMA_CELL_VS_B_LYMPHOCYTE_DN	30	1.38	< 0.0001
KEGG_B_CELL_RECEPTOR_SIGNALING_PATHWAY	63	1.38	< 0.0001
V$XBP1_01	89	-1.63	< 0.0001
SHAFFER_IRF4_TARGETS_IN_ACTIVATED_DENDRITIC_CELL	50	-1.32	< 0.0001
SHAFFER_IRF4_TARGETS_IN_PLASMA_CELL_VS_MATURE_B_LYMPHOCYTE	57	-1.48	< 0.0001
SHAFFER_IRF4_TARGETS_IN_MYELOMA_VS_MATURE_B_LYMPHOCYTE	87	-1.29	< 0.0001
V$PAX5_01	99	1.24	0.0840
BIOCARTA_NFkB_PATHWAY	22	1.39	< 0.0001

Figure 6. Plasma cell transcription signatures in cMYC/KRAS12V-transduced plasmacytoma cells. (**a**) Expression of selected genes from microarray results were confirmed using quantitative real-time PCR. All data represent mean of triplicate experiments. (**b**) GSEA showed a plasma cell gene expression signature of plasmacytoma cells. (**c**) GSEA showed genes associated with B-cell receptor signaling to be significantly downregulated in plasmacytoma cells. (**d**) GSEA showed genes in IRF4 target gene set were upregulated in plasmacytoma cells. (**e**) Table of the gene sets related to plasma cell differentiation and survival.

EZH2,[42] NRF2[43] and YAP[44] (Figure 7d). These results provide further insight into the role of cMYC/KRAS12V in plasmacytoma pathogenesis and identify potential therapeutic targets.

Identifying provirus integration sites and altered genes

Single oncogene transgenic MM mouse models may have long disease latency until the development of disease, as additional genetic lesions and/or epigenetic dysregulations in tumor-initiating cells may be required for tumor development.[12,13] In an adoptive model, provirus integration into host genome can alter host-cell gene expression.[45] To determine whether provirus integrations are involved in the pathogenesis in our model, we identified MSCV integration sites using ligation-mediated PCR method. In total, we identified 11 retroviral integration sites in three diseased mice ($n = 3$, 2–4 clones in each tumor sample Figure 8a). The integration sites are not recurrent, and

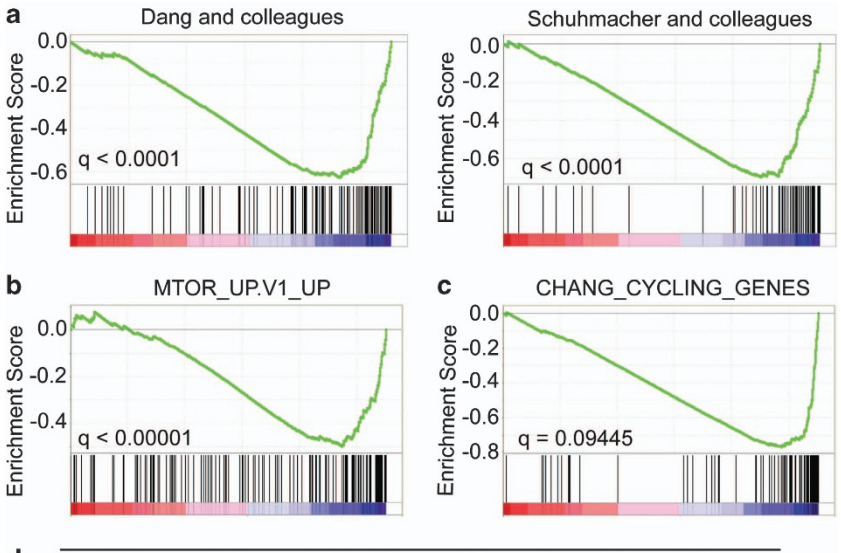

d

Gene Set	SIZE	NES	FDR q-val
DANG_MYC_TARGETS_UP	114	-1.30	< 0.0001
KIM_MYC_AMPLIFICATION_TARGETS_UP	134	-1.27	0.2000
SCHLOSSER_MYC_TARGETS_AND_SERUM_RESPONSE_UP	37	-1.31	< 0.0001
SCHUHMACHER_MYC_TARGETS_UP	67	-1.23	< 0.0001
MTOR_UP.V1_UP	139	-1.49	< 0.0001
MTOR_UP.N4.V1_DN	102	1.43	< 0.0001
CHANG_CYCLING_GENES	100	-1.34	0.09445
SCIAN_CELL_CYCLE_TARGETS_OF_TP53_AND_TP73_DN	22	-1.55	< 0.0001
REN_BOUND_BY_E2F	50	-1.24	0.12277
EGUCHI_CELL_CYCLE_RB1_TARGETS	19	-1.10	0.20000
REACTOME_CELL_CYCLE_MITOTIC	234	-1.36	0.16666
PRC2_EZH2_UP.V1_UP	125	-1.87	< 0.0001
NFE2L2.V2	255	-1.85	< 0.0001
GCNP_SHH_UP_LATE.V1_UP	146	-1.80	0.0138
CORDENONSI_YAP_CONSERVED_SIGNATURE	48	-1.55	0.0734

Figure 7. Gene expression signatures of cMYC/KRAS12V-transduced plasmacytoma cells. (**a**) Using GSEA, four gene sets associated with MYC activation are presented in plasmacytoma cells compared with IgM^+ B cells. (**b**) GSEA showed genes upregulated by mTOR in plasmacytoma cells. (**c**) GSEA showed that genes regulating cell cycle are significantly enriched in plasmacytoma cells. (**d**) Table of gene sets of MYC, mTOR, cell cycle and cancer-related pathways (from top to bottom) in cMYC/KRAS12V-transduced plasmacytoma cells.

there is no evidence indicating an association with MM (Figure 8b). These data indicate that the plasmacytomas derived by MSCV-cMYC/KRAS12V did not require additional genetic lesions.

DISCUSSION

Here we report a rapid-onset high-penetrance mouse model of plasmacytoma based on enforced expression of both cMYC and KRAS12V in T2 B subset population cells via retroviral transduction, followed by transplantation into lethally irradiated mice. The disease latency was about 7 weeks, all recipients developed disease, and most recipients died within 10 weeks. Compared with transgenic models, this adoptive model significantly reduces both time and cost and provides a highly efficient system to evaluate oncogenes. Moreover, it is feasible to combine oncogenes to study their cooperation effects. Conversely, we can introduce RNA-interfering techniques to suppress the expression of specific targets associated with oncogenes. This rapid model therefore provides a faithful *in vivo* system to functionally evaluate the genetic lesions in cancer, both elucidating pathogenesis and evaluating therapeutic targets.

We selected cMYC and KRAS12V as examples to examine the possibility that enforced expression of oncogenes in a specific B-cell population could model plasmacytoma in mice. Deregulated activity of cMYC is highly associated with MM,[26] and previous transgenic mouse models and chemically induced plasmacytomas in BALB/c mice have demonstrated the roles of cMYC in the development of plasmacytomas.[46] KRAS as a secondary oncogene was selected as KRAS mutations can suppress cMYC-induced apoptosis in rat fibroblasts via PI3K/AKT signaling, and KRAS mutations are frequently detected in MM.[36] Moreover, previous studies showed that KRAS12V could enhance cMYC-induced apoptosis via constitutively activating Raf pathway in rat fibroblasts.[36] Of note, v-myc and v-raf had synergistic roles in plasmacytomas in BALB/c mice induced by pristine priming,[21,47] suggesting that the role of Raf signaling might vary with cell types or genetic backgrounds. As expected, KRAS12V efficiently suppressed cMYC-induced apoptosis in a pre-B-cell line (murine BaF3 cells) *in vitro* and successfully induced plasmacytomas *in vivo* by cooperating with cMYC. Finally, in our adoptive mouse model, neither cMYC nor KRAS12V alone was sufficient to induce plasmacytomas in BALB/c mice. Previous transgenic mouse models already indicate that secondary mutations are required for the development of plasmacytomas contributing to their long latency time.[13] Here, we provide KRAS12V as a required secondary gene lesion, which significantly reduces disease latency time.

a

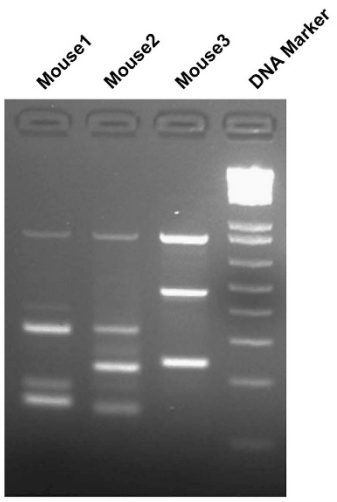

b

MSCV integration sites in plasmacytomas

	Gene	Location and distance	Orientation of provirus	Mouse chromosome
Mouse 1	Rbfox3	Intron 2-3	Inverse	chr:11 118802250
	Acox3	Intron 6-7	Inverse	chr:5 35591691
	Fat1	Intron 25-26	same	chr:8 45047822
	Mfhas1	Intron 1-2	same	chr:8 35616636
	Pkd1l2	Intron 14-15	Inverse	chr:8 117052454
Mouse 2	Thsd7b	3', 210.6kb	Inverse	chr1: 129220192
	Gm12128	3', 243.6kb	Inverse	chr:11 37916770
	Calb1	Intron 9-10	Inverse	chr:4 15903038
	Galnt2	Intron 1-2	same	chr:8 124266283
Mouse 3	Zfp407	Intron 4-5	Inverse	chr:18 84375802
	Sfi1	5', 12.4kb	same	chr 11 3201397

Figure 8. Provirus integration sites. (**a**)The splinkerette-PCR results of provirus integration sites. The lanes of 3% agarose gel showed the splinkerette-PCR production for three mouse plasmacytoma samples with 100 bp marker. Each band represents a provirus integration site and a tumor cell subclone, except for the top band, which represents retroviral vector endogenous fragment (617 bp, not including the linker sequence). (**b**) Identification of MSCV integration sites in plasmacytoma cells.

The target cell population is critical for successful induction of plasmacytoma in recipients. Purified splenic IgM^+ population includes immature B cells, early transitional B cells (T1 B cells), later transitional B cells and memory B cells.[23] After stimulation with LPS and mIL4, the major cell population transits to T2 B-cell subset ($IgM^+B220^+CD38^+IgD$). In this model, T2 B cells were transformed by cMYC/KRAS12V and induced plasmacytoma *in vivo* based on both cell morphology and cell surface biomarkers ($CD138^+B220^-IgM^-GFP^+$). Gene profiling also indicated that tumor cells acquire plasma cell and lose IgM^+ B-cell gene expression signatures. Specifically, plasma cell differentiation genes were significantly upregulated, whereas B-cell-specific transcription factors were repressed. These results are consistent with previous gene profiling studies comparing plasma cells with IgM^+ B cells.[29]

Although the adoptive mouse model does not accurately reflect all the features of human MM, it recapitulates many major characteristics of the disease. In our cMYC/KRAS12V-induced plasmacytoma mouse model, some mice developed hind limb paralysis with plasma cell infiltration of the spine. Histological examination of femur also showed tumor cell infiltration at multiple loci in BM. The lack of lytic bone lesions observed with micro-CT may be associated with lethal irradiation[48] or could be manifested at later points of time. Other MM features, such as hyperglobulinemia and renal injury, were mimicked in this model.

After secondary transplantation of cMYC/KRAS12V-induced plasmacytomas, all recipients developed disease at short latency, 21 days post transplantation compared with 70 days primary transplantation recipients. The major disease features of secondary transplant recipients resemble those in primary transplant recipients. Thus, secondary transplant recipients may represent an even more suitable system for preclinical drug evaluations.

Previous studies have demonstrated that chemically induced plasmacytoma are mouse strain specific.[49] Consistent with these findings, we find that BALB/c, but not C57BL/6, mice are susceptible to cMYC/KRAS12V-induced plasmacytoma. This provides us a way to investigate the role of tumor-suppressor genes in MM pathogenesis, such as P53 and RB1. For example, in both human MM and murine plasmacytoma, loss of function of P53 or RB1 is commonly observed. Thus, our model could be used to determine whether P53 or RB1 has a critical role in preventing the development of cMYC/KRAS12V-induced plasmacytoma.

In summary, this adoptive plasmacytoma mouse model faithfully reflects most of the major characteristics of MM in patients. It affords a system to evaluate the oncogenic events in MM, elucidate mechanism of these events and identify potential targets for future therapy. It will also be useful to study microenvironmental and epigenetic factors in MM, as well as assess potential targeted therapies.

CONFLICT OF INTEREST

The authors declare no conflict of interest.

ACKNOWLEDGEMENTS

We thank Weihua Song, Teru Hideshima and Yu-Tzu Tai for scientific discussion; as well as the Microarray Core and the Flow Cytometry Core Facilities at Dana-Farber Cancer Institute for outstanding technical support. This study was supported in part by National Institutes of Health Grants P50-100707, P01-78378 and RO1-50947. KCA is an American Cancer Society Clinical Research Professor.

REFERENCES

1 Kyle RA, Rajkumar SV. Multiple myeloma. *N Engl J Med* 2004; **351**: 1860–1873.
2 Kuehl WM, Bergsagel PL. Multiple myeloma: evolving genetic events and host interactions. *Nat Rev Cancer* 2002; **2**: 175–187.
3 Bergsagel PL, Kuehl WM. Molecular pathogenesis and a consequent classification of multiple myeloma. *J Clin Oncol* 2005; **23**: 6333–6338.
4 Shaughnessy J, Tian E, Sawyer J, Bumm K, Landes R, Badros A *et al.* High incidence of chromosome 13 deletion in multiple myeloma detected by multiprobe interphase FISH. *Blood* 2000; **96**: 1505–1511.
5 Bergsagel PL, Kuehl WM. Chromosome translocations in multiple myeloma. *Oncogene* 2001; **20**: 5611–5622.
6 Chapman MA, Lawrence MS, Keats JJ, Cibulskis K, Sougnez C, Schinzel AC *et al.* Initial genome sequencing and analysis of multiple myeloma. *Nature* 2011; **471**: 467–472.
7 Anderson PN, Potter M. Induction of plasma cell tumours in BALB-c mice with 2,6,10,14-tetramethylpentadecane (pristane). *Nature* 1969; **222**: 994–995.
8 Urashima M, Chen BP, Chen S, Pinkus GS, Bronson RT, Dedera DA *et al.* The development of a model for the homing of multiple myeloma cells to human bone marrow. *Blood* 1997; **90**: 754–765.
9 Mori Y, Shimizu N, Dallas M, Niewolna M, Story B, Williams PJ *et al.* Anti-alpha4 integrin antibody suppresses the development of multiple myeloma and associated osteoclastic osteolysis. *Blood* 2004; **104**: 2149–2154.
10 Oyajobi BO, Munoz S, Kakonen R, Williams PJ, Gupta A, Wideman CL *et al.* Detection of myeloma in skeleton of mice by whole-body optical fluorescence imaging. *Mol Cancer Ther* 2007; **6**: 1701–1708.
11 Hofgaard PO, Jodal HC, Bommert K, Huard B, Caers J, Carlsen H *et al.* A novel mouse model for multiple myeloma (MOPC315.BM) that allows noninvasive spatiotemporal detection of osteolytic disease. *PLoS One* 2012; **7**: e51892.

12 Chesi M, Robbiani DF, Sebag M, Chng WJ, Affer M, Tiedemann R *et al.* AID-dependent activation of a MYC transgene induces multiple myeloma in a conditional mouse model of post-germinal center malignancies. *Cancer Cell* 2008; **13**: 167–180.
13 Carrasco DR, Sukhdeo K, Protopopova M, Sinha R, Enos M, Carrasco DE *et al.* The differentiation and stress response factor XBP-1 drives multiple myeloma pathogenesis. *Cancer Cell* 2007; **11**: 349–360.
14 Morito N, Yoh K, Maeda A, Nakano T, Fujita A, Kusakabe M *et al.* A novel transgenic mouse model of the human multiple myeloma chromosomal translocation t(14;16)(q32;q23). *Cancer Res* 2011; **71**: 339–348.
15 Cheung WC, Kim JS, Linden M, Peng L, Van Ness B, Polakiewicz RD *et al.* Novel targeted deregulation of c-Myc cooperates with Bcl-X(L) to cause plasma cell neoplasms in mice. *J Clin Invest* 2004; **113**: 1763–1773.
16 Premsrirut PK, Dow LE, Kim SY, Camiolo M, Malone CD, Miething C *et al.* A rapid and scalable system for studying gene function in mice using conditional RNA interference. *Cell* 2011; **145**: 145–158.
17 Cuenco GM, Nucifora G, Ren R. Human AML1/MDS1/EVI1 fusion protein induces an acute myelogenous leukemia (AML) in mice: a model for human AML. *Proc Natl Acad Sci USA* 2000; **97**: 1760–1765.
18 Daley GQ, Van Etten RA, Baltimore D. Induction of chronic myelogenous leukemia in mice by the P210bcr/abl gene of the Philadelphia chromosome. *Science* 1990; **247**: 824–830.
19 Yu D, Thomas-Tikhonenko A. A non-transgenic mouse model for B-cell lymphoma: in vivo infection of p53-null bone marrow progenitors by a Myc retrovirus is sufficient for tumorigenesis. *Oncogene* 2002; **21**: 1922–1927.
20 Zaleskas VM, Krause DS, Lazarides K, Patel N, Hu Y, Li S *et al.* Molecular pathogenesis and therapy of polycythemia induced in mice by JAK2 V617F. *PLoS One* 2006; **1**: e18.
21 Alexander WS, Adams JM, Cory S. Oncogene cooperation in lymphocyte transformation: malignant conversion of E mu-myc transgenic pre-B cells in vitro is enhanced by v-H-ras or v-raf but not v-abl. *Mol Cell Biol* 1989; **9**: 67–73.
22 Xie P, Stunz LL, Larison KD, Yang B, Bishop GA. Tumor necrosis factor receptor-associated factor 3 is a critical regulator of B cell homeostasis in secondary lymphoid organs. *Immunity* 2007; **27**: 253–267.
23 Sanz I, Wei C, Lee FE, Anolik J. Phenotypic and functional heterogeneity of human memory B cells. *Semin Immunol* 2008; **20**: 67–82.
24 Zhang SL, DuBois W, Ramsay ES, Bliskovski V, Morse 3rd HC, Taddesse-Heath L *et al.* Efficiency alleles of the Pctr1 modifier locus for plasmacytoma susceptibility. *Mol Cell Biol* 2001; **21**: 310–318.
25 Silva S, Kovalchuk AL, Kim JS, Klein G, Janz S. BCL2 accelerates inflammation-induced BALB/c plasmacytomas and promotes novel tumors with coexisting T(12;15) and T(6;15) translocations. *Cancer Res* 2003; **63**: 8656–8663.
26 Kobayashi H, Potter M, Dunn TB. Bone lesions produced by transplanted plasma-cell tumors in BALB/c mice. *J Natl Cancer Inst* 1962; **28**: 649–677.
27 Potter M, Fahey JL, Pilgrim HI. Abnormal serum protein and bone destruction in transmissible mouse plasma cell neoplasm (multiple myeloma). *Exp Biol Med* 1957; **94**: 327–333.
28 Korbet SM, Schwartz MM. Multiple myeloma. *J Am Soc Nephrol* 2006; **17**: 2533–2545.
29 Underhill GH, George D, Bremer EG, Kansas GS. Gene expression profiling reveals a highly specialized genetic program of plasma cells. *Blood* 2003; **101**: 4013–4021.
30 Shaffer AL, Lin KI, Kuo TC, Yu X, Hurt EM, Rosenwald A *et al.* Blimp-1 orchestrates plasma cell differentiation by extinguishing the mature B cell gene expression program. *Immunity* 2002; **17**: 51–62.
31 Piskurich JF, Lin KI, Lin Y, Wang Y, Ting JP, Calame K. BLIMP-I mediates extinction of major histocompatibility class II transactivator expression in plasma cells. *Nat Immunol* 2000; **1**: 526–532.
32 Lin Y, Wong K, Calame K. Repression of c-myc transcription by Blimp-1, an inducer of terminal B cell differentiation. *Science* 1997; **276**: 596–599.
33 Schlosser I, Holzel M, Hoffmann R, Burtscher H, Kohlhuber F, Schuhmacher M *et al.* Dissection of transcriptional programmes in response to serum and c-Myc in a human B-cell line. *Oncogene* 2005; **24**: 520–524.
34 Schuhmacher M, Kohlhuber F, Holzel M, Kaiser C, Burtscher H, Jarsch M *et al.* The transcriptional program of a human B cell line in response to Myc. *Nucleic Acids Res* 2001; **29**: 397–406.
35 Zeller KI, Jegga AG, Aronow BJ, O'Donnell KA, Dang CV. An integrated database of genes responsive to the Myc oncogenic transcription factor: identification of direct genomic targets. *Genome Biol* 2003; **4**: R69.
36 Kauffmann-Zeh A, Rodriguez-Viciana P, Ulrich E, Gilbert C, Coffer P, Downward J *et al.* Suppression of c-Myc-induced apoptosis by Ras signalling through PI(3)K and PKB. *Nature* 1997; **385**: 544–548.
37 Zoncu R, Efeyan A, Sabatini DM. mTOR: from growth signal integration to cancer, diabetes and ageing. *Nat Rev Mol Cell Biol* 2011; **12**: 21–35.
38 Majumder PK, Febbo PG, Bikoff R, Berger R, Xue Q, McMahon LM *et al.* mTOR inhibition reverses Akt-dependent prostate intraepithelial neoplasia through regulation of apoptotic and HIF-1-dependent pathways. *Nat Med* 2004; **10**: 594–601.
39 Chang HY, Sneddon JB, Alizadeh AA, Sood R, West RB, Montgomery K *et al.* Gene expression signature of fibroblast serum response predicts human cancer progression: similarities between tumors and wounds. *PLoS Biol* 2004; **2**: E7.
40 Ren B, Cam H, Takahashi Y, Volkert T, Terragni J, Young RA *et al.* E2F integrates cell cycle progression with DNA repair, replication, and G(2)/M checkpoints. *Genes Dev* 2002; **16**: 245–256.
41 Eguchi T, Takaki T, Itadani H, Kotani H. RB silencing compromises the DNA damage-induced G2/M checkpoint and causes deregulated expression of the ECT2 oncogene. *Oncogene* 2007; **26**: 509–520.
42 Bracken AP, Dietrich N, Pasini D, Hansen KH, Helin K. Genome-wide mapping of Polycomb target genes unravels their roles in cell fate transitions. *Genes Dev* 2006; **20**: 1123–1136.
43 Malhotra D, Portales-Casamar E, Singh A, Srivastava S, Arenillas D, Happel C *et al.* Global mapping of binding sites for Nrf2 identifies novel targets in cell survival response through ChIP-Seq profiling and network analysis. *Nucleic Acids Res* 2010; **38**: 5718–5734.
44 Cordenonsi M, Zanconato F, Azzolin L, Forcato M, Rosato A, Frasson C *et al.* The Hippo transducer TAZ confers cancer stem cell-related traits on breast cancer cells. *Cell* 2011; **147**: 759–772.
45 Coffin JMHS, Varmus HE. *Retrovirus*. Cold Spring Harbor Laboratory Press: Cold Spring Harbor, NY, USA, 1997.
46 Potter M, Wiener F. Plasmacytomagenesis in mice: model of neoplastic development dependent upon chromosomal translocations. *Carcinogenesis* 1992; **13**: 1681–1697.
47 Kurie JM, Morse 3rd HC, Principato MA, Wax JS, Troppmair J, Rapp UR *et al.* v-myc and v-raf act synergistically to induce B-cell tumors in pristane-primed adult BALBC mice. *Oncogene* 1990; **5**: 577–582.
48 Seed TM, Chubb GT, Tolle DV. Sequential changes in bone marrow architecture during continuous low dose gamma irradiation. *Scanning Microsc* 1981; **4**: 61–72.
49 Zhang S, Ramsay ES, Mock BA. Cdkn2a, the cyclin-dependent kinase inhibitor encoding p16INK4a and p19ARF, is a candidate for the plasmacytoma susceptibility locus, Pctr1. *Proc Natl Acad Sci USA* 1998; **95**: 2429–2434.

Supplementary Information accompanies this paper on Blood Cancer Journal website (http://www.nature.com/bcj)